Available online at www.sciencedirect.com
ScienceDirect
Thermochimica Acta 469 (2008) 12–22
thermochimica acta
www.elsevier.com/locate/tca

Thermal decomposition of ammonium paratungstate tetrahydrate under non-reducing conditions Characterization by thermal analysis, X-ray diffraction and spectroscopic methods

M.J.G. Fait [a], H.-J. Lunk [b,*], M. Feist [c], M. Schneider [a], J.N. Dann [b], T.A. Frisk [b]

[a] *Berlin Branch of Leibniz Institute for Catalysis at Rostock University, Richard-Willstätter-Str. 12, D-12489 Berlin, Germany*
[b] *OSRAM Sylvania, Hawes Street, Towanda, PA 18848, USA*
[c] *Humboldt-Universität zu Berlin, Institut für Chemie, Brook-Taylor-Str. 2, D-12489 Berlin, Germany*

Received 13 November 2007; received in revised form 30 November 2007; accepted 9 December 2007
Available online 28 December 2007

Abstract

The thermal decomposition of ammonium paratungstate tetrahydrate (APT·$4H_2O$), $(NH_4)_{10}[H_2W_{12}O_{42}]\cdot 4H_2O$, in air to tungsten trioxide, WO_3, was investigated under non-isothermal conditions using thermal analysis coupled on-line by a *Skimmer*® system to a quadrupole mass spectrometer (TA-MS) for evolved gas analysis (EGA), with X-ray powder diffraction (XRD), with Fourier transform infrared (FT-IR) and Raman spectroscopy. The decomposition is characterized by three endothermic and one exothermic step. The first endothermic step comprises the release of crystal water resulting in the formation of crystal-water-free ammonium paratungstate. During the second endothermic step ammonia is released leaving behind ammonium hydrogen paratungstate, $(NH_4)_6H_4[H_2W_{12}O_{42}]$. The presence of protons in the "roasted" APT was supported by *ex situ* and *in situ* FT-IR spectroscopy (vibration bands at 1100 and 2160 cm^{-1}). Ammonium hydrogen paratungstate is the precursor for the metatungstate anion, $[H_2W_{12}O_{40}]^{6-}$, which is formed during the digestion of "roasted" APT with hot water.

Keywords: Ammonium paratungstate; Ammonium metatungstate; Tungsten trioxide; Thermal decomposition

1. Introduction

Monoclinic ammonium paratungstate tetrahydrate, $(NH_4)_{10}[H_2W_{12}O_{42}]\cdot 4H_2O$, which will be referred to as APT·$4H_2O$, is widely used as the industrial feedstock for the production of tungsten carbide, WC (cf. e.g. [1]), for the powder metallurgical production of tungsten filaments (cf. e.g. [2]), for various tungsten heavy alloys (cf. e.g. [3]) and also as starting material for producing ammonium metatungstate (AMT), $(NH_4)_6[H_2W_{12}O_{40}]\cdot\sim 3H_2O$, which is utilized in the catalyst industry (cf. e.g. [4]).

The centrosymmetric paratungstate 'Z' anion $[H_2W_{12}O_{42}]^{10-}$ of APT·$4H_2O$ [5] consists of four corner-sharing W_3O_{13} groups and two non-acidic protons. Every W_3O_{13} group consists of three edge-sharing WO_6 octahedra (Fig. 1a). The distance between the two non-acidic protons was determined by broad-line ^1H NMR spectroscopy as 2.22 Å [6]. Later on, this result was confirmed by neutron diffraction experiments [7]. Therefore, the formula $(NH_4)_{10}[H_2W_{12}O_{42}]\cdot 4H_2O$ is a better representation of the structure than the out-dated, but still used formula $(NH_4)_{10}W_{12}O_{41}\cdot 5H_2O$.

Tungsten(VI) oxide, WO_3, can be used as an oxidizing catalyst (e.g. oxidizing propene and furan [8]). It is also a component of mixed metal oxides, e.g. of the type $Mo_{1-x}(V, W)_xO_{3-y}$, which are employed as catalysts for the partial oxidation of light alkenes [9]. Due to its wide usage, the thermal decomposition of APT·$4H_2O$ under non-reducing, reducing or oxidizing conditions is still a focus of investigation. As demonstrated by studies in nitrogen, air or hydrogen [10–16], APT·$4H_2O$ decomposes at temperatures up to about 380 °C independently of the atmosphere used, liberating ammonia and water. The decomposition was studied using temperature-programmed *in situ* techniques like XRD, spectroscopic (IR, DRS, EXAFS) and thermoanalytical (TG-DTA, DSC) as well as other methods to monitor the

* Corresponding author. Tel.: +1 570 268 5503; fax: +1 570 268 5350.
E-mail address: hans-joachim.lunk@sylvania.com (H.-J. Lunk).

0040-6031/$ – see front matter © 2008 Elsevier B.V. All rights reserved.
doi:10.1016/j.tca.2007.12.007

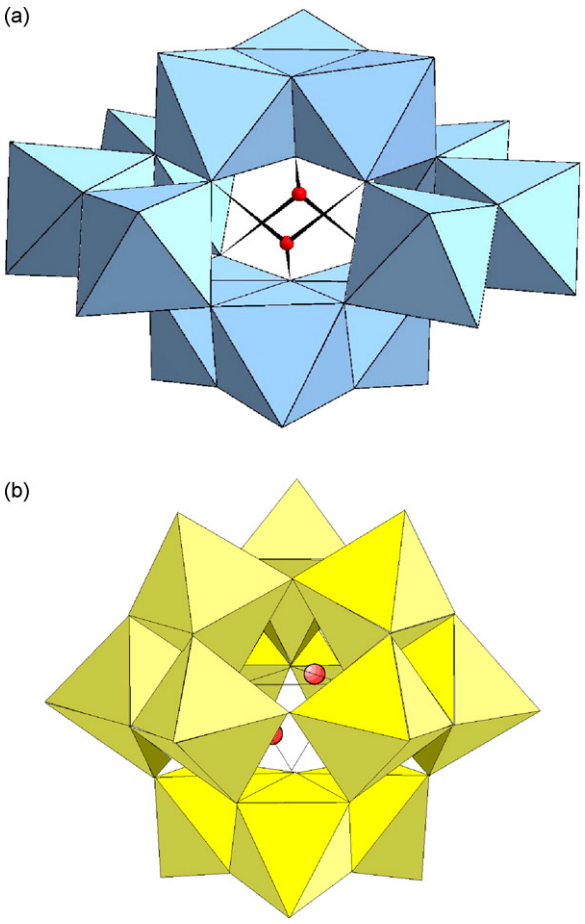

Fig. 1. (a) Polyhedral representation of the paratungstate 'Z' anion $[H_2W_{12}O_{42}]^{10-}$ and (b) Polyhedral representation of the metatungstate anion $[\alpha\text{–}H_2W_{12}O_{40}]^{6-}$ (so-called α–Keggin-anion).

evolved gases. At about 400 °C re-crystallization occurs, which can be detected by its exothermic effect. Above 400 °C various reactions take place, depending on the experimental conditions. In an oxidizing atmosphere yellow WO_3 is formed. Tungsten trioxide exists as triclinic, monoclinic, orthorhombic, and tetragonal crystal systems, which are all distortions of the well-known cubic ReO_3 structure with corner-shared WO_6 octahedra (Fig. 2a).

The hexagonal WO_3 modification [17] has the same framework as the hexagonal alkali metal tungsten bronzes, also based on corner-shared WO_6 octahedra, this time with six-sided empty tunnels (Fig. 2b).

Under inert (mostly N_2) or reducing conditions (H_2 or H_2/N_2 mixtures) tungsten blue oxide (TBO), $x\mathrm{NH_3}\cdot y\mathrm{H_2O}\cdot\mathrm{WO}_n$, is produced. The term 'tungsten blue oxide' does not describe a well-defined compound, but is the designation of a blue-colored product manufactured industrially from APT·$4H_2O$. Different TBOs contain varying amounts of crystalline components and X-ray amorphous phases [18].

There is no doubt that the decomposition of APT·$4H_2O$ proceeds via different intermediates. However, the definite identification of these phases is still a matter of discussion. Due to the lack of information about relevant parameters of the starting material (actual crystal water content, concentration of trace elements, bulk density, sieve analysis, sample size, bed height), a comparison of literature data is often difficult or even impossible to make.

The overall thermal decomposition of APT·$4H_2O$ in air into tungsten trioxide can be described by the simplified equation:

$$(NH_4)_{10}[H_2W_{12}O_{42}]\cdot 4H_2O \rightarrow 4H_2O + 1H_2O + n\mathrm{NH_3} + \{\mathrm{NH_3} + 0.5H_2O\}_{10-n} + n/2H_2O + 12WO_3 \quad (1)$$

as the stepwise release of the four molecules of crystal water, the release of the structural water, the release of just NH_3, the release of NH_3/H_2O (see Eq. (2)) mixtures, and finally the release of the remaining water.

$$(NH_4)_2O \rightarrow 2\mathrm{NH_3} + H_2O \quad (2)$$

This process (see Eq. (2)) proceeds while using up oxide ions from the paratungstate anion.

As repeatedly confirmed by the studies of others, the first step of the APT·$4H_2O$ decomposition is the release of crystal water. However, the end temperature for this event varies from 100 °C [10,11] to 170 °C [19,20]. According to Ref. [10],

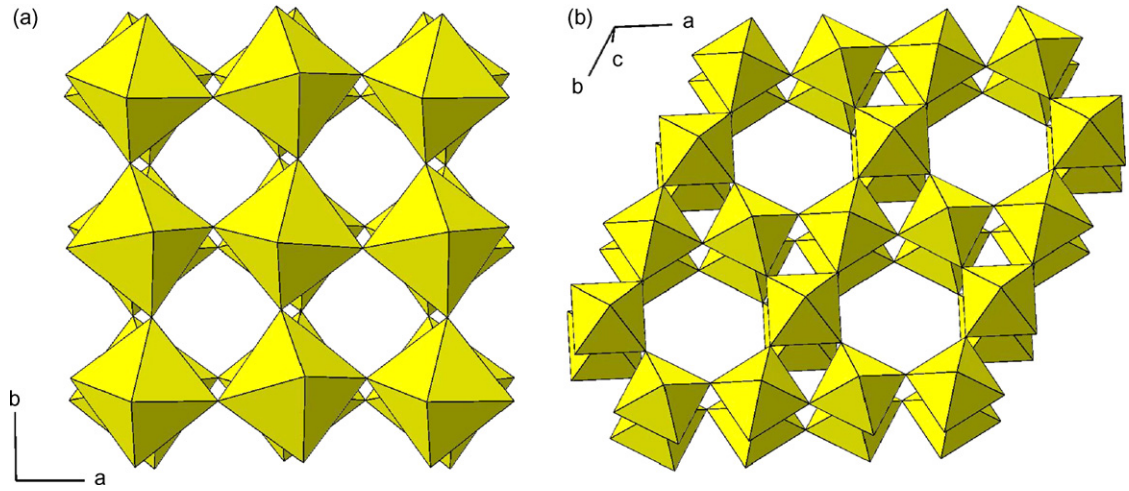

Fig. 2. Polyhedral representations of tungsten trioxide WO_3 (a) Triclinic modification (distorted cubic ReO_3 structure) and (b) Hexagonal modification.

the initially formed anhydrous ammonium paratungstate is believed to undergo the transformation to "amorphous ammonium metatungstate dihydrate", while releasing ammonia. In the temperature range from 220 to 320 °C "amorphous ammonium tungstate" is believed to be formed, while ammonia and water are liberated simultaneously. The entire process is completed at 500 °C [10].

The formation of ammonium paratungstate monohydrate was detected by Ref. [19] as the first decomposition step at 100 °C, followed by the generation of polytungstates with various stoichiometric compositions from 100 to 280 °C. According to Ref. [21], between 100 °C and approximately 220 °C, only NH_3 is evolved and amorphous ammonium metatungstate is formed. In another study, crystalline ammonium metatungstate was observed at 210 °C [22]. The recent publications [23,24] describe the decomposition of APT·$4H_2O$ in oxidizing and non-oxidizing atmospheres using several characterization methods specifically for tracing the evolved gases. However, the phase changes, including the formation of intermediates in the temperature range up to ca. 300 °C, are referred to only briefly.

APT·$4H_2O$ decomposes into an X-ray amorphous phase, which eventually crystallizes into WO_3. Its crystallization is detected by an exothermic effect in the DTA experiment, whereas the preceding release of volatile ammonia and water is accompanied by several endothermic effects. In Ref. [22] a strong exothermic effect at 265 °C was reported, which later was interpreted as combustion of ammonia [24].

The question of which WO_3 modification is formed in oxidizing atmosphere during the APT·$4H_2O$ decomposition was studied in a few publications. According to Ref. [25], the monoclinic WO_3 phase is formed first, which is transformed at 800 °C into the tetragonal modification. Alternatively, Refs. [24,26] suggest that prior to the WO_3 formation in nitrogen and air, a crystallization process must take place resulting in the formation of hexagonal ammonium tungsten bronze, $(NH_4)_nWO_3$ ($0 < n \leq 0.33$).

The aim of this study is to reinvestigate the thermal decomposition of APT·$4H_2O$ to tungsten trioxide under non-reducing conditions. Special attention was paid to the detection of relevant intermediates with reduced amounts of ammonia and water. The thermal effects based on simultaneously coupled EGA measurements will be discussed in relation to the stoichiometry of the compounds formed and compared to XRD and FT-IR results. Both methods were performed using *in situ* and *ex situ* techniques. In addition, Raman spectroscopy was employed. The results presented here are the basis of a kinetic analysis of the APT·$4H_2O$ decomposition, which will be published.

2. Experimental

APT·$4H_2O$ from OSRAM Sylvania used in this study was characterized as shown in Table 1. TA-MS analysis was performed using a thermal analyzer STA 409C (Netzsch Gerätebau GmbH, Selb/Germany), which was coupled to a quadrupole mass spectrometer (QMG 422, Balzers). The conditions were: 70 mL min^{-1} air flow, 5 K min^{-1} heating rate, about 200 mg sample mass, corundum crucibles. Platinum crucibles were used for comparison. The overlapping individual steps have been distinguished by their minima in the DTG curve. The ion current (IC) curves for the selected ions with $m/z = 15$ (NH^+), 17 (OH^+; $NH_3{}^+$), and 18 (H_2O^+) were recorded in the multiple ion detection (MID) mode. Analogously to the heating regime of the *in situ* XRD measurements, stepwise isothermal TA-MS experiments (e.g. temperature holds at 100, 150, 200, 250, 300, 350, 400, 450, 500, 550, 700, and 750 °C for 50 min) were performed in air (about 70 mL min^{-1}). Each TA-MS experiment has been repeated at least two times.

Table 1
Characterization of $(NH_4)_{10}[H_2W_{12}O_{42}]\cdot 2.5H_2O$

Trace element	Al	As	Ca	Cr	Cu	Fe	K	Na	Mg	Mn	Mo	Ni	P	Si	Sn	Ta
ppm	1	<5	<1	<1	<1	1	<2	6	<1	<1	<6	<1	<7	<1	1	<20

Sieve analysis

Mesh	<40	<60	<100	<200	<325
%	100	99	89	43	23

Bulk density: 42.2 g/in^3 (2.57 g/cm^3).

The *in situ* XRD data were collected using a theta–theta diffractometer (Seifert-FPM Germany) with multilayer and "quasi parallel geometry", fixed slit, Cu Kα1 radiation, 2θ range of 5–50°, step size of 0.02°, dwell time of 1 s/step resulting in a hold time of 3.3 min at the respective temperature. The powdered sample was placed on a horizontal Pt–Rh sample holder (HDKS1 heating chamber, Bühler) and heated from 100 to 650 °C (heating rate 2.5 K min^{-1}) in an airflow of 100 mL min^{-1}. Prior to the measurements the sample holder was coated with gold to suppress the well-known catalytic activity of Pt–Rh for the oxidation of ammonia (see Section 3.3).

The *in situ* FT-IR spectra were recorded on a BRUKER IFS 66 spectrometer from a self-supporting disc (100 mg, without KBr) placed in a heatable IR cell (5 K min^{-1} heating rate, 50 mL min^{-1} air flow, KBr windows, dispersion 2 cm^{-1}). In the course of the thermal decomposition this disc lost its mechanical stability and, hence, the maximum recorded temperature was 300 °C.

Only the *in situ* measurements TA-MS, XRD and FT-IR provide first-hand information about the decomposition process of APT·$4H_2O$. All other methods applied are dealing with a situation where the substances were exposed to the ambient conditions prior to the measurement.

The *ex situ* XRD data were collected using a D/max-vertical diffractometer from RIGAKU, with parafocusing geometry, graphite monochromator, fixed slits (divergence slit = scatter slit = 1°), and Cu Kα radiation. Scanning conditions were 6–70° 2Θ, step size of 0.02°, and a dwell time of 2 s/step.

The following X-ray powder diffraction reference files from the ICDD [27] were used.

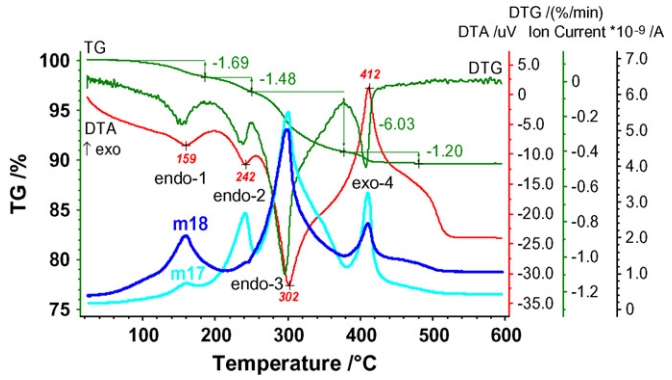

Fig. 3. TA-MS curves of the decomposition of $(NH_4)_{10}[H_2W_{12}O_{42}]\cdot 2.5H_2O$ in air with the ion current curves for $m/z = 17$ (NH_3^+; OH^+) and 18 (H_2O^+) (heating rate: 5 K min^{-1}).

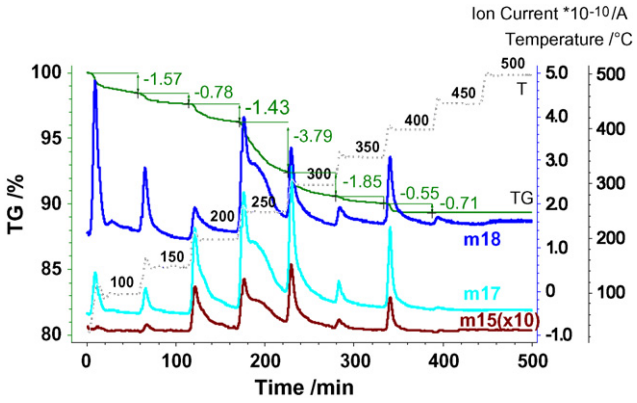

Fig. 5. TA-MS curves of the decomposition of $(NH_4)_{10}[H_2W_{12}O_{42}]\cdot 2.5H_2O$ in air with the ion current curves for $m/z = 15$ (NH^+), 17 (NH_3^+; OH^+) and 18 (H_2O^+) (analogously to *in situ* XRD measurements).

Phase	ICDD PDF	System	Space group
$(NH_4)_{10}[H_2W_{12}O_{42}]\cdot 4H_2O$	00–040–1470	Monoclinic	$P2_1/n$ (14)
$(NH_4)_6[H_2W_{12}O_{40}]\cdot 20H_2O$	00–039–0186	Cubic	
$(NH_4)_{0.33}WO_3$	00–042–0452	Hexagonal	
WO_3	04–005–4301	Triclinic	P-1 (2)
WO_3	04–005–4272	Monoclinic	$P2_1/n$ (14)
WO_3	04–007–2425	Orthorhombic	$Pcnb$ (60)
WO_3	04–007–2426	Tetragonal	$P4/ncc$(130)
WO_3	04–007–2322	Hexagonal	$P6_3/mcm$ (193)

The *ex situ* FT-IR spectra were recorded on a NICOLET Magna 760 spectrometer. The samples were diluted with KBr in a mass ratio of 1:15. The mixture was analyzed using diffuse reflectance infrared Fourier-transform (DRIFT) spectroscopy. Pure KBr was used to acquire the background signal. Number of sample scans: 256; resolution: 4000; laser frequency: 473 THz; detector: DTGS; beamsplitter: KBr.

The Raman spectra were recorded on a NICOLET 590 Raman Accessory. Samples were analyzed neat within NMR tubes. Number of sample scans: 512; resolution: 4000; laser frequency: 473 THz, Raman laser frequency 281 THz; detector: InGaAs; beamsplitter: CaF_2; Raman laser power: 0.09 W.

3. Results and discussion

The thermal decomposition of the starting ammonium paratungstate in air is represented by the TA-MS curves in Fig. 3. Four mass loss steps accompanied by three endothermic (endo-1, endo-2, and endo-3) and one exothermic effect (exo-4) can be recorded. The individual steps overlap implying certain consequences when regarding the phase composition reached for each step after either dynamic or isothermal (see below) mode. An inspection of the evolution of the IC intensity ratio between $m/z = 17$ and 18 together with the curve shape for $m/z = 15$ (Fig. 5) yields an interesting description of the general character of the four qualitatively different individual steps. During the first step water and trace amounts of ammonia, iden-

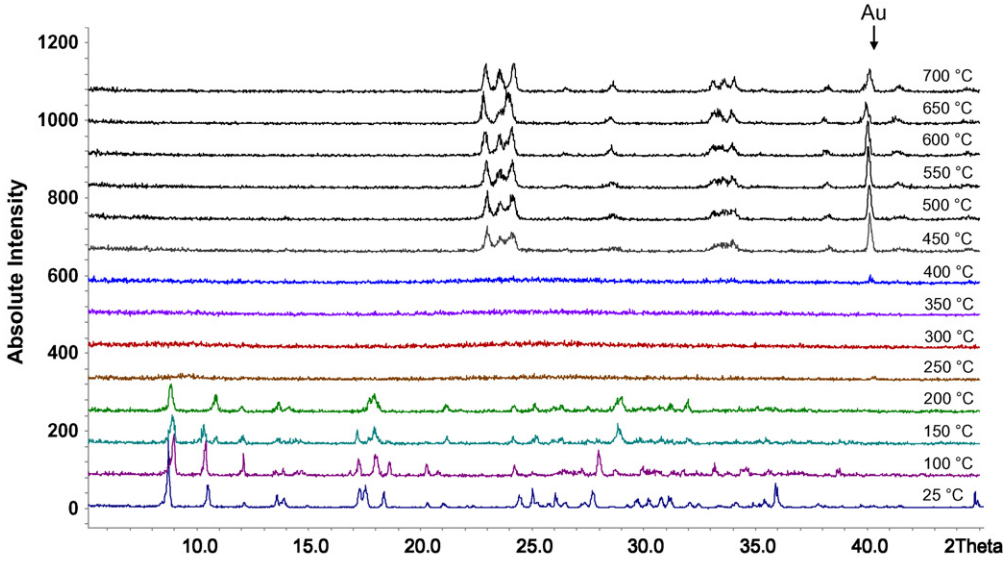

The appearance of the reflection at about 41° identified as gold is caused by "shining through" of the sample holder.

Fig. 4. *In situ* XRD patterns in the course of the thermal decomposition of $(NH_4)_{10}[H_2W_{12}O_{42}]\cdot 2.5H_2O$ in air flow.

Table 2
Thermal decomposition of $(NH_4)_{10}[H_2W_{12}O_{42}]\cdot 2.5H_2O$ in air (cf. Fig. 3)

Step	T/°C	T_P/°C	Δm/%	Δn/mol "$(NH_4)_2O$"[a]	Δn/mol NH_3	Δn/mol H_2O
endo-1	53–186	159	1.69			2.9
endo-2	186–250	242	1.48		2.7	
endo-3	250–377	302	6.03	2.5	1.3	1.35 + 0.65
exo-4	377–480	412	1.20	0.5		0.6
Balance			10.40	3.00	4.0	5.5

T_P peak temperature.
[a] Thermal decomposition according to Eq. (2).

tified in the IC curve for $m/z = 15$ (Fig. 5), are liberated. During the second step only ammonia is liberated. During the third step comparable amounts of ammonia and water evolve, whereas during the fourth step more ammonia than water is released. The second "pure ammonia step" was rather unexpected and prompted a stepwise isothermal TA-MS experiment which precisely followed the thermal regime of the XRD measurement (Fig. 4), i.e. isothermal setting for 50 min at each step (Fig. 5).

The *in situ* XRD patterns generated throughout the thermal decomposition process of APT·2.5H_2O in air (25–650 °C), shown in Fig. 4, allow for an identification of the individual phases formed at each step. Unfortunately, the reciprocal correspondence of the chemical information that may be derived from both methods is not consistent for the whole temperature range investigated. The overlapping of the individual steps, which has been stated already in the dynamic TA experiment, explains that longer annealing causes a greater mass loss for a given temperature than dynamic heating. This is a quite usual experience, which hinders an unambiguous assignment of a mass loss to a phase composition determined by XRD. For the first decomposition step at about 100 °C, the mass loss reached by stepwise heating in TA (1.57%) approximates the value from dynamic TA (1.69%). In the middle temperature range at about 220–250 °C, where the "pure ammonia step" occurred, the neighboring TG steps overlapped and yielded a much greater mass loss (1.57 + 0.78 + 1.43 + 3.79 = 7.59%) than the sum of the dynamic values (1.69 + 1.48 = 3.17%, i.e. a value that would correspond only to dehydration and ammonia loss; cf. Figs. 3 and 5). The cause of this disparity is unknown at this time.

As can be seen from the *T* curve in Fig. 5, a certain overheating (temperature overshoot) is unavoidable when heating to the set temperatures, even by using the useful sample temperature control (STC) function in the manufacturer's software. A very slow heating rate for the setting, on the other hand, possibly could avoid the small *T* jumps at the beginning of an isothermal plateau. However, it cannot prevent the progression of the decomposition during the setting ramp from one TG step to the next. The overshooting of the temperature target at the beginning of an isothermal step causes the unusual signal shape of the IC curves, which limited the understanding of the reactions in the middle temperature range.

For the total mass loss, of course, the situation is different. Both for the dynamic treatment up to 500 °C and for the stepwise heating, the mass losses are nearly the same (10.40 vs. 10.68%). The total mass loss of most APT lots produced by OSRAM Sylvania varied between 10.60 and 10.70% with an average of 10.63%, which corresponds to 2.83 mol crystal water per APT formula.

Thus, the overall mass loss of 10.40–10.68% of the sample studied corresponds to 2.5–2.9 mol crystal water per formula $(NH_4)_{10}[H_2W_{12}O_{42}]$, which represents a deficit of 1.5–1.1 mol crystal water compared to the filled structure with 4 mol H_2O. As the starting material crystallized in the structure of APT·4H_2O, which was confirmed by its XRD pattern (Fig. 4 and Table 3), the APT·4H_2O structure obviously "tolerates" the loss of 1.5 H_2O without any structural changes. The stoichiometry, however, cannot deviate from the ratio of 10 NH_4^+ cations per paratungstate anion $[H_2W_{12}O_{42}]^{10-}$ due to electron neutrality. The formula $(NH_4)_{10}[H_2W_{12}O_{42}]\cdot 2.5H_2O$ (APT·2.5H_2O) will be used throughout the remainder of this study.

In the following the four individual steps of the APT·2.5H_2O decomposition identified by dynamic TA are discussed in relation to the TA-MS, *in situ* XRD and also spectroscopic measurements.

3.1. First step: endo-1 (50–190 °C)

The first endothermic step in the temperature range of 50 to 190 °C is characterized by a mass loss of 1.69% (Fig. 3). The strong signal of the H_2O^+ curve ($m/z = 18$) (Fig. 3) implies the release of water which corresponds to 2.9 mol crystal water (Table 2) and is in good agreement with the formula of APT·2.5H_2O. The rate of crystal water release reaches its maximum at 159 °C (Table 2). Under dynamic conditions no ammonia formation could be detected, but the steps at 100 and 150 °C in the corresponding isothermal TA-MS experiment (Fig. 5) show a very low IC intensity in the IC curve for $m/z = 15$ representing ammonia ($^{14}NH^+$; $^{15}N^+$). This ammonia evolution might be interpreted in terms of being transported with the water. The main character of the first decomposition step of APT·2.5H_2O is undoubtedly the formation of the anhydrous ammonium paratungstate, $(NH_4)_{10}[H_2W_{12}O_{42}]$, which agrees with the literature [10].

According to the isothermal TA-MS measurement (Fig. 5) the mass loss of 1.57% at 100 °C corresponds to the release of 2.7 mol H_2O and the formation of $(NH_4)_{10}[H_2W_{12}O_{42}]\cdot\sim 0H_2O$. Compared with the dynamic experiment (Fig. 3), the stage of anhydrous ammonium paratungstate is reached at lower temperatures by the isothermal technique. A shift to lower temperatures was observed also for all the other thermal effects.

Table 3
Major reflections of X-ray data for the starting APT·2.5H_2O, samples heated up to 100, 150 and 200 °C and also for three AMT hydrates

APT (*in situ* XRD)								AMT (*ex situ* XRD)					
2.5H_2O		Heated to 100 °C		Heated to 150 °C		Heated to 200 °C		20H_2O		~3H_2O		~0H_2O	
2Θ (°)	I_{rel} (%)	2Θ (°)	I_{rel} (%)	2Θ (°)	I_{rel} (%)	2Θ (°)	I_{rel} (%)	2Θ (°)	I_{rel} (%)	2Θ (°)	I_{rel} (%)	2Θ (°)	I_{rel} (%)
8.73	100	8.97	100	8.89	100	8.83	100	7.9	4	6.9	5	6.9	7
10.49	36	10.39	85	10.23	43	10.81	55	8.5	26	9.5	100	9.6	92
12.10	8	12.10	52	10.32	71	12.01	21	8.8	100	10.0	98	10.0	100
13.58	20			10.88	30	13.69	36	9.6	4	10.3	19		
17.29	30	17.24	42	17.18	52	14.14	20	9.8	4	15.2	7	15.3	6
17.55	33			17.91	49	17.71	42	10.0	17	16.5	56	16.7	50
18.38	24	17.98	51			17.96	62	16.5	18	17.2	18	17.2	21
		18.06	48			21.15	29	17.1	6	17.5	22	17.6	29
24.43	20					24.28	25	17.3	19	17.9	18	17.9	18
25.03	27			25.17	30	25.14	31	18.5	15	19.1	32	19.1	25
26.05	21					26.32	26	19.5	12	20.0	35	20.0	33
27.71	25	27.98	60	28.84	61	28.81	50	19.8	27	20.4	37	20.6	37
35.89	37					28.96	49	19.9	34				
44.81	24					31.97	29						

The XRD pattern of the starting material APT·2.5H_2O matches APT·4H_2O (PDF 00–40–1470) (Table 3). The diffractogram at 100 °C exhibits significant changes of the main reflections. The strongest reflection is shifted from 8.73° to 8.97°. The reflection at 10.49° remains nearly unchanged and appears at 10.39° (85%). The reflection at 2Θ = 12.10° becomes stronger (8 → 52%). Whereas the reflections at 2Θ = 17.29° and 17.55° merge to one reflection at 17.24° (42%), the reflection at 18.38° splits into two reflections at 17.98° (51%) and 18.06° (48%). The reflection at 27.71° is slightly shifted to 27.98° (60%).

The crystal water has been completely released as can be seen on the TG-MS profile in the dynamic as well as in the isothermal experiment. A similar conclusion can be drawn for a series of published *in situ* XRD patterns in a temperature range up to 175 °C. These diffractograms reflect the formation of APT hydrates with decreasing amounts of crystal water; no details about the stoichiometries have been specified [15].

The diffraction angles and reflection intensities of the XRD pattern at 150 °C (Fig. 4 and Table 3) are quite different from that of anhydrous APT observable at 100 °C. It will be discussed in the following section because it is comparable to that, which was obtained at 200 °C.

3.2. Second step: endo-2 (190–250 °C)

The second step endo-2 in the temperature range 190–250 °C is characterized by a mass loss of 1.48% and a DTA peak temperature of 242 °C (Fig. 3 and Table 2).

Unambiguously, this step is caused by the release of ammonia. However, ammonia can be liberated by two alternative routes; as a 2NH_3:1H_2O mixture formed according to Eq. (2), or as NH_3 formed alone according to Eq. (3)

$$NH_4^+ \rightarrow NH_3 + H^+ \quad (3)$$

The simultaneous release of ammonia and water would use up oxide ions from the paratungstate anion, thereby leading to the gradual destruction of its structure. The following experimental results verify that the cation NH_4^+ is stripped of NH_3 leaving behind the proton H^+.

(i) The IC intensity for $m/z = 18$ representing H_2O^+ (Fig. 3) is not zero due to tailing in the gas phase. No distinct peak in the IC curve for $m/z = 18$ was detected, but a significant intensity for $m/z = 17$ was recorded. Furthermore, the IC maximum coincides with a separate DTA peak at 242 °C, thus representing a distinct process. Obviously, the ammonia formation is not accompanied by a dehydration process. The same tendency was observed in the isothermal experiment (Fig. 5). Note that during the isothermal steps at 100 and 150 °C, the intensity ratio of the mass numbers $m/z = 17$ and 18 confirms the liberation of water at these steps. During the 200 °C step, the $m/z = 17$ intensity exceeds that of $m/z = 18$, indicating that also ammonia is released at this step. The $m/z = 15$ intensity is also much greater at this step than the corresponding intensities for the previous two steps. This is clearly due to the release of ammonia. Other than for the dynamic experiment, the two stages at 200 and 250 °C in the stepwise heating do not represent a "pure ammonia step", as expected.

(ii) In the *in situ* FT-IR spectrum (Fig. 6), recorded with the same heating rate as the TA-MS measurement, a band appeared at 1110 cm^{-1} in the temperature range 175–275 °C. Its intensity reached its maximum at 225 °C, then remained constant up to 275 °C and decreased to zero at 300 °C. This behavior is in agreement with the developing of the IC curve for $m/z = 17$ (Fig. 3). Its maximum intensity coincides with the DTA peak temperature of 242 °C. The band at 1110 cm^{-1} might be ascribed to a hydrogen bond between two neighboring terminal oxygen atoms (O_t) of the paratungstate anion W-O_t···H^+···O_t-W.

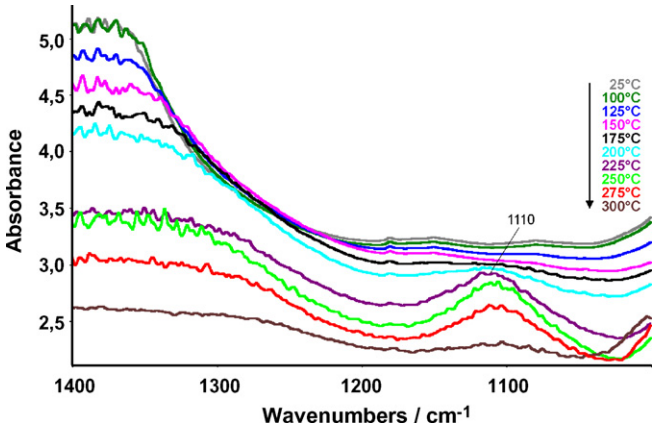

Fig. 6. *In situ* FT-IR spectra of $(NH_4)_{10}[H_2W_{12}O_{42}]\cdot 2.5H_2O$ in the course of heating in air flow (heating rate: 5 K min^{-1}).

Most likely, during the stripping process "naked" protons are formed (Eq. (3)).

(iii) Samples of about 80 mg were heated in the *in situ* XRD cell (cf. Section 2) in air up to 100, 150, 200 and 250 °C, respectively. After holding the samples at the selected temperature for 15 min, they were cooled down to room temperature and then stored under ambient conditions. As a result the primarily formed proton H^+ was hydrated to the oxonium ion H_3O^+. The *ex situ* FT-IR spectra of the starting material and of the sample heated to 100 °C are identical (Fig. 7). The spectra of the samples heated up to 150 and 200 °C revealed four new bands at 1096 (strong), 1640 (weak), 2160 (strong), and 3440 cm^{-1} (weak). According to Ref. [28], the bands at 1640 and 2160 cm^{-1} are due to H_3O^+. The band at 2160 cm^{-1} might be assigned to an overtone of the deformation band at 1096 cm^{-1} [29].

(iv) Ammonium metatungstate, AMT·∼$3H_2O$, is produced in a commercial process by "roasting" APT·$4H_2O$ in air in the temperature range from 260 to 315 °C, then digesting the raw product with hot water and spray drying the aqueous solution [30]. Lots of APT·$4H_2O$ roasted under manufacturing conditions at various temperatures and then exposed to the ambient conditions was characterized by chemical analysis, *ex situ* XRD and *ex situ* FT-IR spectroscopy. The XRD patterns reveal that the structure of APT·$4H_2O$, characterized by a molar ratio of $10NH_3$:$12WO_3$, is still present for APT·$4H_2O$ heated up to 250 °C with overall NH_3:$12WO_3$ ratios of 7.70, 7.00, 6.09 and 5.76, respectively. The degree of crystallinity (ratio of peak area above the background curve to the total area) of these samples, however, is reduced from 80% for the starting APT·$2.5H_2O$ down to 55, 50, 35 and finally 25% for the $5.76NH_3$:$12WO_3$ sample. Fig. 8 exhibits the *ex situ* FT-IR spectra of these five samples. The four absorption bands at 1096 (strong), 1640 (weak), 2160 (strong), and 3450 cm^{-1} (weak) are assigned in the same way as for the samples under (iii). The overall formulae $7.70NH_3\cdot 12WO_3\cdot 9.25H_2O$ and $7.00NH_3\cdot 12WO_3\cdot 9.43H_2O$ can be written as $(NH_4)_{7.70}(H_3O)_{2.30}[H_2W_{12}O_{42}]\cdot 0.95H_2O$ and $(NH_4)_{7.00}(H_3O)_{3.00}[H_2W_{12}O_{42}]\cdot 0.43H_2O$, implying the hydration of H^+ to H_3O^+ during the exposure of the samples to ambient conditions. The intensity of the four bands is considerably reduced for the sample with 6.09 NH_3 and even more for the composition $5.76NH_3$:$12WO_3$.

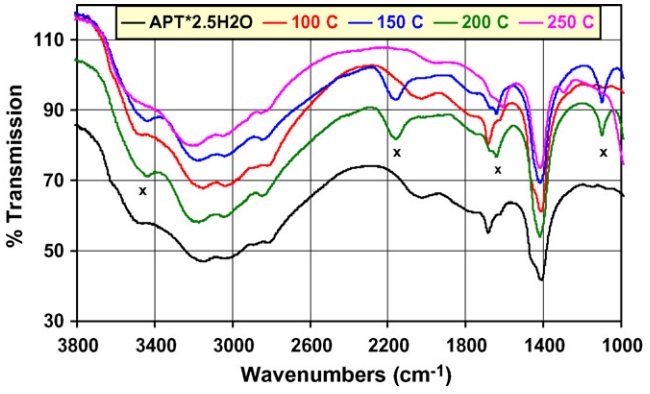

Fig. 7. *Ex situ* FT-IR spectra of starting APT·$2.5H_2O$ and of samples heated in an *in situ* XRD cell at 100, 150, 200, and 250 °C. Asterisks indicate the new bands.

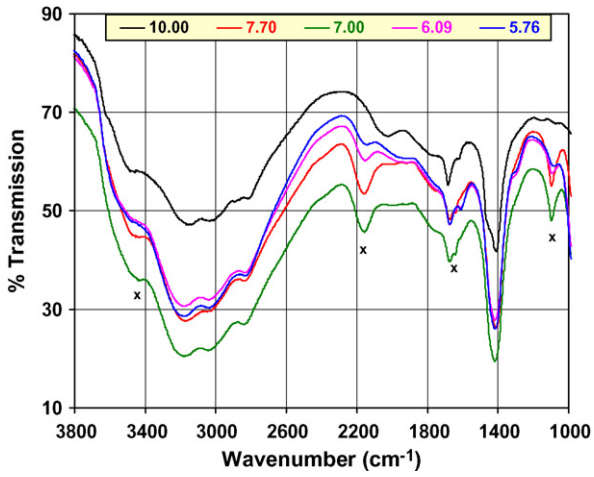

Fig. 8. *Ex situ* FT-IR spectra of starting APT·$2.5H_2O$ and samples heated under manufacturing conditions up to 250 °C $(NH_4)_{10}[H_2W_{12}O_{42}]\cdot 2.50H_2O$ (10.00), $7.70NH_3\cdot 12WO_3\cdot 9.25H_2O$ (7.70), $7.00NH_3\cdot 12WO_3\cdot 9.43H_2O$ (7.00), $6.09NH_3\cdot 12WO_3\cdot 7.58H_2O$ (6.09), $5.76NH_3\cdot 12WO_3\cdot 7.27H_2O$ (5.76). Asterisks indicate the new bands.

For eight roasted APT samples with the overall compositions $n$$NH_3$:$12WO_3$ ($5.76 \le n \le 7.70NH_3$), the ratio of the intensity of the band at 2160 cm^{-1} to the band at 1096 cm^{-1} remains constant at 2.15 with a S.D. of 0.17.

By flushing the sample $7.70NH_3$:$12WO_3$ with dry ammonia gas, in a noticeably exothermic reaction the starting composition $10NH_3$:$12WO_3$ could be restored (cf. Fig. 9). The alternative method of "re-ammoniating" the stripped APT is by keeping the sample for 2 days in a desiccator over concentrated aqueous solution of ammonia. (cf. Fig. 9). As expected, the hydration alone of the sample $7.70NH_3$:$12WO_3$ virtually did not change its FT-IR spectrum (cf. Fig. 9).

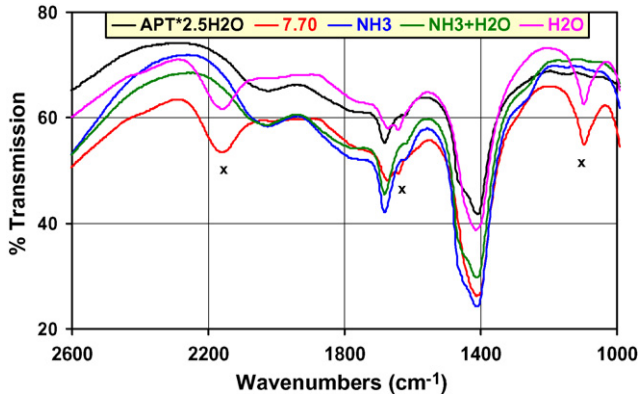

Fig. 9. *Ex situ* FT-IR spectra: $(NH_4)_{10}[H_2W_{12}O_{42}]\cdot 2.50H_2O$ (APT·2.5H_2O). Addition of dry ammonia gas to $7.70NH_3\cdot 12WO_3\cdot 9.25H_2O$ (7.70) resulting in $9.74NH_3\cdot 12WO_3\cdot 9.05H_2O$ (NH_3) or of ammonia and water to $7.70NH_3$ resulting in $10.29NH_3\cdot 12WO_3\cdot 8.31H_2O$ (NH_3 + H_2O). The hydration alone of sample $7.70NH_3$ resulted in $7.46NH_3\cdot 12WO_3\cdot 10.86H_2O$ (H_2O). Asterisks indicate the new bands.

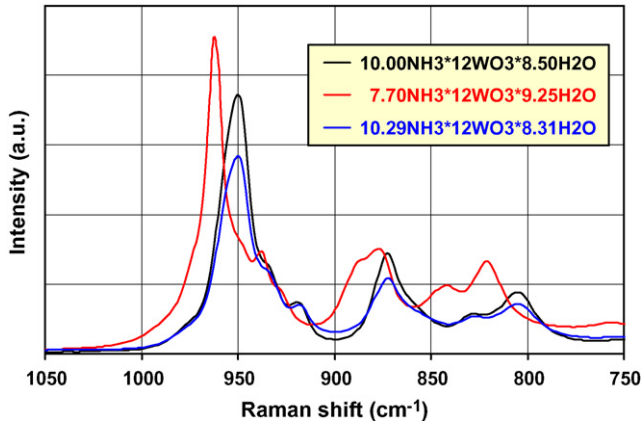

Fig. 10. Raman spectra of APT·2.5H_2O ($10.00NH_3\cdot 12WO_3\cdot 8.50H_2O$), compared to $7.70NH_3\cdot 12WO_3\cdot 9.25H_2O$ and "ammoniated" $10.29NH_3\cdot 12WO_3\cdot 8.31H_2O$.

The Raman spectra (Fig. 10) document that stripping 2.3 mol NH_3 per APT formula resulted in a $\sim$15 cm^{-1} bathochromic shift of all absorption bands, which is completely reversed after neutralizing the 2.3 mol protons with ammonia.

It can be concluded from these findings that the structure of the paratungstate anion remains generally unchanged during the endothermic step endo-2. The mass loss of 1.48% (Table 2) is attributed to the release of 2.7 mol NH_3, disregarding the formation of traces of water during this step.

In summary, the step endo-2 is characterized by the release of predominately NH_3, leaving behind protons and keeping the paratungstate anion unchanged according to the following Eq. (4):

$$(NH_4)_{10}[H_2W_{12}O_{42}] \rightarrow 2.7NH_3 + (NH_4)_{7.3}H_{2.7}[H_2W_{12}O_{42}] \quad (4)$$

The *in situ* X-ray powder patterns observed at 150 and 200 °C (Fig. 4 and Table 3) match neither the cubic AMT·20H_2O (PDF 00-039-0186) nor OSRAM Sylvania's spray-dried AMT·$\sim$3H_2O, which is stable under standard conditions (Fig. 11 and Table 3). AMT·20H_2O left in air, will effloresce and turn into stable AMT·$\sim$3H_2O. Spray-dried AMT·$\sim$3H_2O stored in a vacuum desiccator over P_4O_{10} for several days will lose water and turn into anhydrous AMT, whose diffractogram resembles that of AMT·$\sim$3H_2O (Fig. 11 and Table 3). We could not confirm the findings of others [10,22]

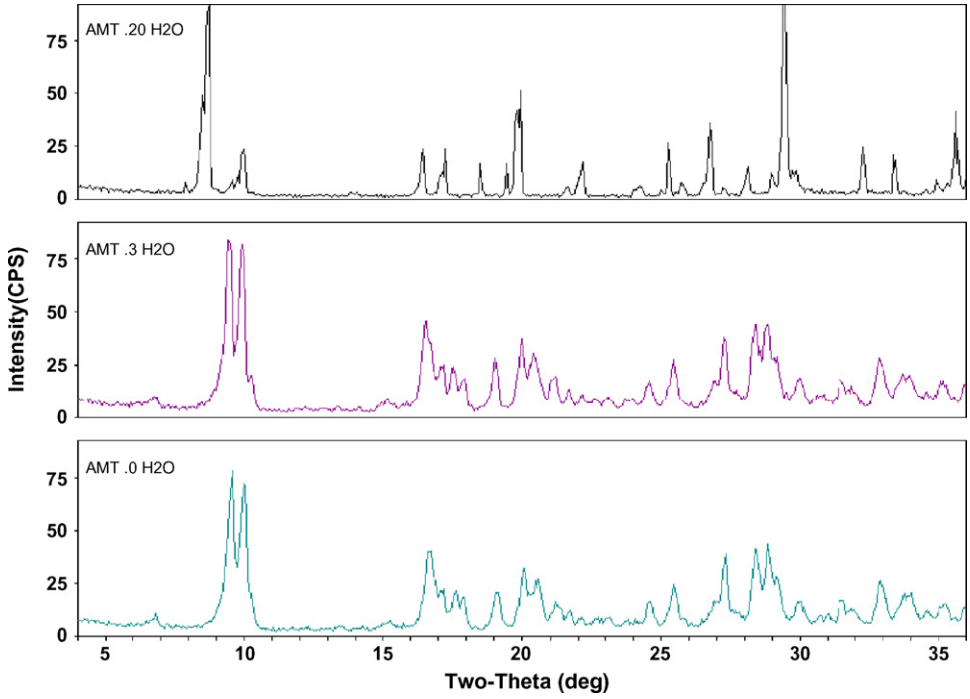

Fig. 11. *Ex situ* XRD patterns of the 20-, 3-hydrates and the crystal-water-free ammonium metatungstate $(NH_4)_6[H_2W_{12}O_{40}]\cdot nH_2O$ (n = 20, 3, 0).

that AMT is an intermediate phase formed during the thermal decomposition of anhydrous APT followed by the formation of an X-ray amorphous phase. Based on our test work under laboratory and manufacturing conditions, we could demonstrate that the metatungstate anion, $[H_2W_{12}O_{40}]^{6-}$, is formed only during digesting roasted APT with hot water. A composition of the roasted material as close as possible to $(NH_4)_6H_4[H_2W_{12}O_{42}]$ results in the maximum yield of $[H_2W_{12}O_{40}]^{6-}$. Formally, the polycondensation of the paratungstate anion to the metatungstate anion during the digestion process can be described as follows:

$$[H_2W_{12}O_{42}]^{10-} + 4H^+ \rightarrow [H_2W_{12}O_{40}]^{6-} + 2H_2O \quad (5)$$

The structure of the metatungstate anion $[H_2W_{12}O_{40}]^{6-}$ is based on a central tetrahedron surrounded by 12 WO_6 octahedra arranged in four groups of three edge-shared octahedra, W_3O_{13} (cf. Fig. 1b). The distance between the two non-acidic protons in the center of the anion was determined by broad-line ^{1}H NMR spectroscopy as 1.92 Å [6].

3.3. Third step: endo-3 (250–380 °C)

The third endothermic step in the temperature range 250–380 °C (T_P = 302 °C) is associated with a mass loss of 6.03% (Table 2). In contrast to step endo-2, the gas released is a mixture of NH_3 and H_2O, based on the curve shape of the IC curves for m/z = 17 and 18 (Fig. 3). In the isothermal experiment (Fig. 5) the IC curves for m/z = 15, 17, and 18 at 200 °C are very similar. Their shape is comparable with that of the m/z = 17 curve in the dynamic mode. However, the thermal event proceeds at a temperature, about 50 K lower, as mentioned above. The shape of the m/z = 17 curve in the dynamic operation mode indicates that ammonia is released in two steps with different rates.

Next, the stoichiometric changes (Table 2) are discussed, as they relate to the relative portions of ammonia and water. Due to the lack of quantitative IC curves for ammonia and water, the interpretation of the data is tentative. The 2.7 mol H^+ formed during step endo-2 are released as 1.35 mol H_2O. An additional 1.3 mol NH_3 {10 mol − 2.7 mol (endo-2) − 1.3 mol (endo-3) = 6 mol} is liberated leading to the formation of $(NH_4)_6H_4[H_2W_{12}O_{42}]$ (cf. Section 3.2), followed by the corresponding release of 0.65 mol H_2O (cf. Eq. (2)). The 2.5 mol $(NH_4)_2O$ (5 mol NH_3, 2.5 mol H_2O) balances the overall mass loss of 6.03% of step endo-3. The NH_3 balance of 2.7 mol (endo-2) + 6.3 mol (endo-3) = 9.0 mol reveals a deficit of 1 mol compared to the total of 10 mol NH_3. Hence, the remaining 1 mol NH_3 must be released during the final step exo-4.

During step endo-3 the main portion of ammonia is released, which requires the consumption of oxide ions from the decomposing paratungstate anion (Eq. (2)). As a result, the destruction of the polyoxoanion is progressing, leading to a completely X-ray amorphous phase as detected in the temperature range 250–400 °C (Fig. 4). This was also confirmed by an *in situ* XAFS study [15]. The signals showed a small amplitude in the range between 2 and 4 Å indicating a significant loss of structural order. However, we cannot agree with the given identification of the intermediate as hexagonal ammonium tungsten bronze, $(NH_4)_nWO_3$ ($n \leq 0.33$). We assume that under the chosen experimental conditions hexagonal WO_3 was formed.

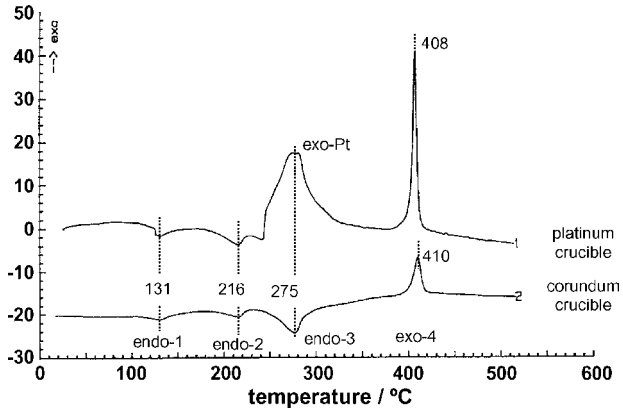

Fig. 12. DTA curves of $(NH_4)_{10}[H_2W_{12}O_{42}]\cdot 2.5H_2O$ in air using different crucibles.

The liberation of gaseous ammonia and water causes the collapse of the remaining structural fragments, which, according to the XAFS study, leads to low-ordered WO_6 entities [15].

In contrast to our findings, a strong exothermic effect in the temperature range 200–400 °C was observed in Ref. [10,22,24]. According to the MS-EGA experiments, this result was explained as oxidation of NH_3 to nitrous gases catalyzed by the products formed during the APT decomposition [24]. The exothermic effect could be observed only when platinum crucibles were used [24]. To confirm the literature data, $APT\cdot 2.5H_2O$ was decomposed under identical conditions using a corundum crucible to compare it with the behavior in platinum (Fig. 12). In the case of the corundum crucible, an endothermic peak endo-3 at 275 °C was observed, whereas in platinum, a distinct exothermic effect (exo-Pt) emerged (T_P = 275 °C). This temperature coincides with the IC maximum of ammonia evolved. Taking into account the MS-EGA results from Ref. [24], the findings can be explained unambiguously as the combustion of NH_3 to nitrous gases, catalyzed by platinum, which basically corresponds to the industrial "OSTWALD process".

3.4. Fourth step: exo-4 (>380 °C)

In contrast to the other three steps, the thermal step exo-4 above 380 °C is accompanied by an exothermic effect associated with a mass loss of 1.20% (Fig. 3 and Table 2). The peak temperature at 412 °C of the DTA trace coincides with the DTG peak and the IC maxima for NH^+ and H_2O^+. But the whole exothermic reaction is more extensive than the TG step alone, encompassing a range of over 150 °C. Obviously, the heat evolution caused by the crystallization of WO_3 far outweighs the endothermic gas release.

The mass loss is caused by the liberation of an overall amount of 1.1 mol H_2O and 1.0 mol NH_3. However, the water evolved originates from different sources: 0.5 mol stems from the decomposition of remaining 0.5 mol $(NH_4)_2O$ (Eq. (2)), 0.6 mol H_2O are "structural water" formed from the two non-acidic protons

located in the center of the original paratungstate anion. The discrepancy of 0.4 mol compared to 1 mol structural water per $[H_2W_{12}O_{42}]^{10-}$ can be explained by the slight differences in the cursor position (DTG minimum between two overlapping signals) when the partial steps in a TG curve are graphically separated.

Integration of the IC curves for $m/z = 15$ for the three signals endo-2, endo-3 and exo-4 (derived from APT·2.5H_2O decomposition in argon under identical conditions as in the experiment in air, not shown) provides a peak area ratio of 1:5.39:1.82 leading to a molar NH_3 ratio of 1.2:6.6:2.2. These values agree roughly with the ratio of 2.7:6.3:1.0 derived from stoichiometric calculations (Table 2). This result confirms the proposed decomposition steps from APT·2.5H_2O to WO_3. The crystallization of WO_3 is an exothermic reaction with the related DTA peak temperature at 412 °C and the corresponding XRD pattern appearing at 450 °C.

The very low intensity diffraction peak at $2\Theta = 14°$, observable at 450 and 500 °C (cf. Fig. 4), suggests the possibility of the existence of a hexagonal phase. The authors [26] postulated that hexagonal ammonium tungsten bronze was formed. Alternatively, the formation of hexagonal WO_3 is possible. The structures of hexagonal ammonium tungsten bronze and h-WO_3 are closely related. Based on the TA-MS measurement (Fig. 3) alone it is impossible to decide which phase is formed. Nevertheless, it is very unlikely that hexagonal ammonium tungsten bronze is formed under oxidizing conditions. In addition, the available quantity of ammonia, if any, is too small for stabilizing this phase.

Due to the low crystallinity of WO_3, formed at 450 °C, its X-ray diffractogram cannot be unambiguously assigned to either the monoclinic or orthorhombic modification. The thermodynamically stable phase at room temperature is monoclinic WO_3, which transforms to the orthorhombic modification at 467 °C [31]. Therefore, at 450 °C it is probably the monoclinic modification which is formed, as was postulated by other authors [25,32].

4. Conclusions

The thermal decomposition of ammonium paratungstate tetrahydrate was studied under non-reducing conditions in the temperature range 25–600 °C using thermal analysis and X-ray powder diffraction and IR spectroscopy, both techniques in *ex situ* and *in situ* modes. The APT decomposition is characterized by a sequence of three endothermic and one exothermic step. Special attention has been paid to the characterization of the products formed at these four steps.

It is unambiguous that during the first step the anhydrous ammonium paratungstate, $(NH_4)_{10}[H_2W_{12}O_{42}]$, is formed.

Mass spectroscopy, IR and Raman spectroscopy confirmed, for the first time, that during the second endothermic step ammonia alone is released leaving behind protons under formation of ammonium hydrogen paratungstate, $(NH_4)_6H_4[H_2W_{12}O_{42}]$. The paratungstate ion remains generally unchanged during the release of NH_3. In this course $(NH_4)_6H_4[H_2W_{12}O_{42}]$ constitutes the precursor for the metatungstate ion, $[H_2W_{12}O_{40}]^{6-}$, which is only formed during digesting roasted APT with hot water. The subsequent crystallization from the mother liquor or spray-drying the aqueous solution results in the formation of $(NH_4)_6[H_2W_{12}O_{40}]\cdot nH_2O$.

During the third endothermic step the main portion of gas is released as a mixture of NH_3 and H_2O, which requires the consumption of oxide ions from the decomposing paratungstate anion. This results in a completely X-ray-amorphous phase.

The decomposition is finished by the fourth step, which is accompanied by the release of remaining ammonia/water and structural water. The exothermic heat effect of this step is caused by the formation of tungsten trioxide, WO_3, detectable by XRD.

Applying the knowledge gained from studying APT decomposition, especially for the second endothermic step, to the production of AMT under manufacturing conditions resulted in a significant increase in AMT yield.

Acknowledgements

The authors are grateful to U. Bentrup, J. Spandl and T. Dang for valuable discussion of the FT-IR spectra, to U. Wolf and H.J. Stevens for technical assistance and to H. Hartl for providing the polyhedral representations.

References

[1] P.K. Mehrotra, K.P. Mizgalski, A.T. Santhanam, Int. J. Powder Metall. 43 (2007) 33–40.
[2] J.L. Walter, C.L. Briant, J. Mater. Res. 5 (1990) 2004–2022.
[3] J.R. Davis, in: J.R. Davis (Ed.), ASM Specialty Handbook: Heat-Resistant Materials, ASM International, Materials Park, OH, USA, 1999, pp. 361–382.
[4] X. Zhu, X. Li, X. Zou, Y. Wang, M. Jia, W. Zhang, Catal. Commun. 7 (2006) 579–582.
[5] H. D'Amour, R. Allmann, Z. Kristallogr. 136 (1972) 23–47.
[6] V.I. Spicyn, H.-J. Lunk, V.F. Čuvaev, I.D. Kolli, Z. Anorg. Allg. Chem. 370 (1969) 191–201.
[7] H.T. Evans Jr., E. Prince, J. Am. Chem. Soc. 105 (1983) 4838–4839.
[8] B. Coq, F. Figueras, M. Figlarz, C. R. Acad. Sci. Ser. II 296 (1983) 1229–1232.
[9] B. Grzybowska-Swierkosz, Topics Catal. 11-12 (2000) 23–42.
[10] G.J. French, F.R. Sale, J. Mater. Sci. 16 (1981) 3427–3436.
[11] A.K. Basu, F.R. Sale, J. Mater. Sci. 12 (1977) 1115–1124.
[12] N.E. Fouad, A.K.H. Nohman, M.I. Zaki, Thermochim. Acta 239 (1994) 137–145.
[13] L. Bartha, A. Kiss, J. Neugebauer, T. Nemeth, High Temp. High Pressure 14 (1982) 1–10.
[14] N. Fouad, A. Nohman, M.I. Zaki, Thermochim. Acta 343 (2000) 139–143.
[15] O. Kirilenko, F. Girgsdies, R.E. Jentoft, T. Ressler, Eur. J. Inorg. Chem. (2005) 2124–2133.
[16] I.M. Szilágyi, J. Madarász, F. Hange, G. Pokol, J. Therm. Anal. Calorim. 88 (2007) 139–144.
[17] B. Gerand, G. Nowogrocki, J. Guenot, M. Figlarz, J. Solid State Chem. 29 (1979) 429–434.
[18] H.-J. Lunk, B. Ziemer, M. Salmen, D. Heidemann, Int. J. Refract. Met. Hard Mater. 12 (1993–1994) 17–26.
[19] A.B. Kiss, L. Chudik-Major, Acta Chim. Acad. Sci. Hung. 78 (1973) 237–251.
[20] A.B. Kiss, T. Nemeth, E. Szalanczy, J. Mater. Sci. 13 (1978) 2541–2547.
[21] J.W. van Put, Int. J. Refract. Met. Hard Mater. 13 (1995) 61–76.
[22] S.A.A. Mansour, M.A. Mohamed, M.I. Zaki, Thermochim. Acta 129 (1988) 187–196.
[23] I.M. Szilágyi, M. Janos, F. Hange, P. Gyorgy, Solid State Ionics 172 (2004) 583–586.

[24] J. Madarász, I.M. Szilágyi, F. Hange, G. Pokol, J. Anal. Appl. Pyrolysis 72 (2004) 197–201.
[25] G. Kohlstrung, Phys. Stat. Sol. 2 (1962) 85–96.
[26] Y. Yamamoto, K. Gotani, N. Shigaki, Funtai oyobi Funmatsu Yakin 40 (1993) 609–613.
[27] International Centre for Diffraction Data, 12 Campus Boulevard, Newtown Square, PA, 19073, USA.
[28] G. Mirth, J. Lercher, M. Anderson, J. Klinowski, J. Chem. Soc., Faraday Trans. 86 (1990) 3039–3044.
[29] R. Buzzoni, S. Bordiga, G. Ricchiardi, G. Spoto, A. Zecchina, J. Phys. Chem. 99 (1995) 11937–11951.
[30] V. Chiola, J.M. Laferty Jr., C.D. Vanderpool, US 3,175,881 Sylvania Electric Products Inc. (30.3.1965).
[31] Ph. Labbé, Key Eng. Mater. 68 (1992) 293–340.
[32] Y. Yamamoto, A. Matsumoto, S. Honkawa, N. Shigaki, Funtai oyobi Funmatsu Yakin 40 (1993) 784–788.